LETTERS
PUBLISHED ONLINE: 25 JANUARY 2009 | DOI: 10.1038/NPHYS1182
nature physics

Spin-resolved quantum-dot resonance fluorescence

A. Nick Vamivakas[1*†], Yong Zhao[1,2*], Chao-Yang Lu[1,3] and Mete Atatüre[1†]

Confined spins in self-assembled semiconductor quantum dots promise to serve both as probes for studying mesoscopic physics in the solid state and as stationary qubits for quantum-information science[1–7]. Moreover, the excitations of self-assembled quantum dots can interact with near-infrared photons, providing an interface between stationary and 'flying' qubits. Here, we report the observation of spin-selective photon emission from a resonantly driven quantum-dot transition. The Mollow triplet[8] in the scattered photon spectrum—the hallmark of resonance fluorescence when an optical transition is driven resonantly—is presented as a natural way to spectrally isolate the photons of interest from the original driving field. We also demonstrate that the relative frequencies of the two spin-tagged photon states can be tuned independent of an applied magnetic field through the spin-selective dynamic Stark effect, induced by the same driving laser. This demonstration should be a step towards the realization of challenging tasks such as electron-spin readout, heralded single-photon generation for linear-optics quantum computing and spin–photon entanglement.

In the realm of solid-state emitters generating flying qubits, milestone achievements so far include single-photon antibunching[9,10], entangled photon-pair generation[11] and cavity quantum electrodynamics in the strong coupling regime[12–14]. A common feature in all of these studies is the incoherent pumping of the quantum-dot transitions through carrier generation in either the host matrix such as GaAs or the quasi-continuum states above the higher-lying confined states of the quantum dot. This excitation method leads to photon-emission-time jitter and spectral wandering of the quantum-dot transition larger than the transition's linewidth. Both effects reduce the usefulness of non-resonantly generated single photons in linear-optics quantum computing algorithms[15], even if the quantum dot is coupled to a cavity. In an attempt to both address this previous shortcoming and provide spectrally selective access to the quantum-dot electronic transitions, increasing attention has turned to resonant optical excitation. So far, resonant optical addressing of quantum dots has relied predominantly on a remarkably powerful laser-based spectroscopy technique: differential transmission[16]. Although differential transmission has enabled progress in spin-selective excitation of quantum dots, access to the scattered photons correlated with the quantum-dot spin has proven elusive. Recently, differential transmission and, independently, cavity-assisted temporal correlation measurements have shown clear signatures of dressed-state formation under strong laser light excitation on neutral quantum dots[17–21]. Noting all successful quantum-information science (QIS) implementations on well-developed qubit candidates, such as trapped ions, have relied on spin-selective resonance scattering[22], it is clear that an immediate goal for quantum dots is the observation of the full resonance fluorescence spectrum carrying the desired spin-qubit information.

Coupling two states of a quantum system by a monochromatic laser results in scattered photons with distinct spectral and coherence properties that may be tuned as the properties of the laser (for example, power, frequency and polarization) are varied. Barring any dephasing mechanisms, when the effective Rabi frequency is much less than the spontaneous emission rate, the interference between the scattered photons and the laser field forms the basis of the above-mentioned differential-transmission technique. When the effective Rabi frequency is larger than the spontaneous emission rate, the electronic states are dressed (see Fig. 1a, inset)[23]. The spectrum of the photons scattered in this limit exhibits a multi-Lorentzian structure known as the Mollow triplet[8]—first observed on atomic sodium in 1975 (ref. 24) and as recent as 2007 on a single molecule[25]. The central frequencies for these transitions are:

$$\nu_{\mathrm{red}} = \nu_0 + \Delta - \Omega; \qquad \nu_{\mathrm{central}} = \nu_0 + \Delta; \qquad \nu_{\mathrm{blue}} = \nu_0 + \Delta + \Omega, \tag{1}$$

and the linewidth of each detuned sideband is $(3/2)\gamma_{\mathrm{sp}}$. Here, ν_0 is the bare quantum-dot X^{-1} transition frequency, Δ is the laser frequency detuning from ν_0 (negative for red-detuning) and $\Omega = \sqrt{\Delta^2 + \Omega_{\mathrm{b}}^2}$ (Ω_{b}) is the effective (bare) Rabi frequency.

We start by presenting the observation of the Mollow triplet in the resonance fluorescence spectrum from a single-quantum-dot transition and then proceed to link this with the quantum-dot spin. Figure 1a shows X^{-1} resonance fluorescence spectra on a linear–log scale for a range of laser powers (no external magnetic field). The laser is resonant with the doubly degenerate bare X^{-1} quantum-dot transition frequency. For laser powers above 216 nW, two equal-weight sidebands emerge, which, together with the central feature, constitute the Mollow triplet. The sharp peak in the central feature is residual laser background (see Supplementary Information, Fig. S2). Peak-to-peak sideband splittings determined from this data are plotted in Fig. 1b against the square root of the laser power. In the strong excitation regime ($\Omega_{\mathrm{b}} \geqslant \gamma_{\mathrm{sp}}$), the linear fit confirms the dependence of the sideband splitting on the square root of the laser power.

The observation of the Mollow triplet from a quantum dot should not come as a surprise; however, the measured sideband linewidths are intriguing. Figure 1c shows a linear–linear zoom-in on the Mollow sidebands for a laser power of 1.852 μW ($\Omega_{\mathrm{b}} \approx 8\gamma_{\mathrm{sp}}$). When fitted with the resonance fluorescence spectrum (see Supplementary Information, Discussion), a transition linewidth of 343 (±39) MHz per sideband is extracted, in close agreement with the pure spontaneous emission rate of 227 (±7) MHz obtained from photon-correlation measurements at an excitation power well below saturation. The linewidth places an upper bound of

[1]Cavendish Laboratory, University of Cambridge, JJ Thomson Avenue, Cambridge CB3 0HE, UK, [2]Physikalisches Institut, Ruprecht-Karls-Universität Heidelberg, Philosophenweg 12, 69120 Heidelberg, Germany, [3]HFNL & Department of Modern Physics, University of Science and Technology of China, Hefei, 230026, China. *These authors contributed equally to this work. †e-mail: anv21@cam.ac.uk; ma424@cam.ac.uk.

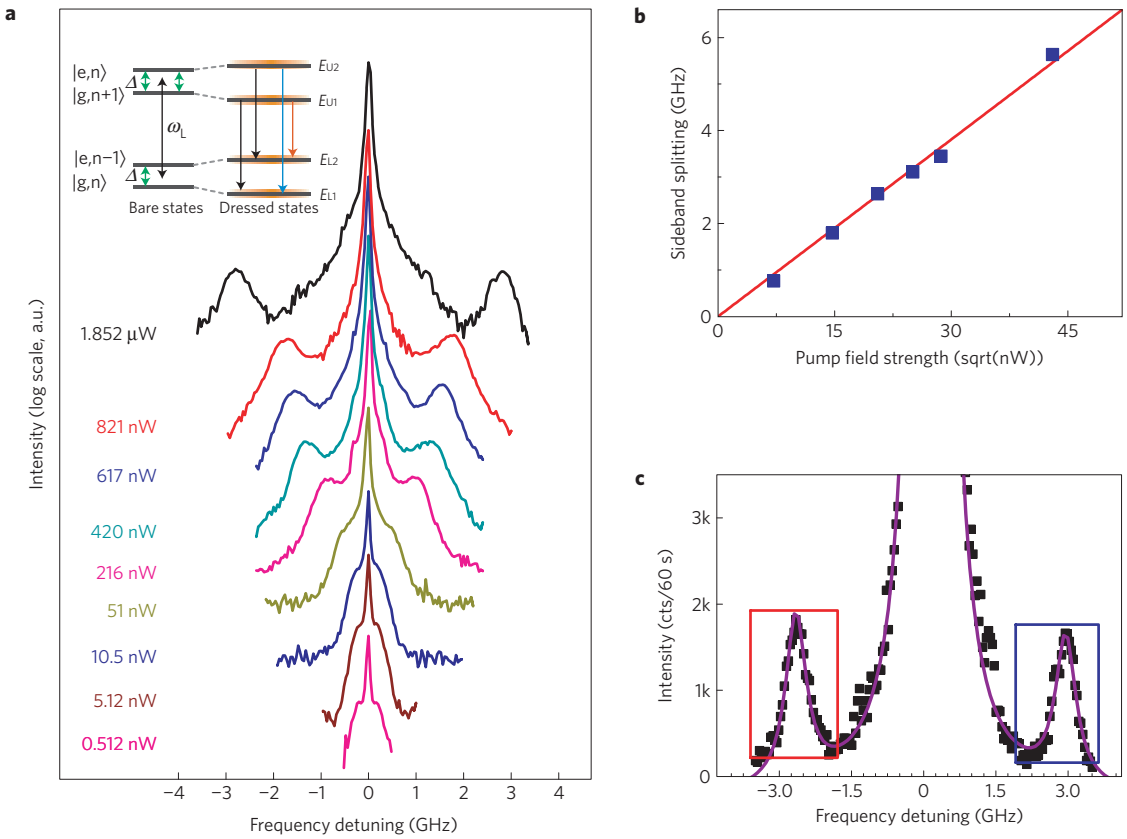

Figure 1 | Power-dependent resonance fluorescence. a, Evolution of the Mollow triplet spectrum as the resonant laser power is increased from 0.512 nW ($\Omega_b \approx 0.13\gamma_{sp}$) to 1.852 μW ($\Omega_b \approx 8\gamma_{sp}$) under zero magnetic field. The intensity of the spectrum is plotted on a logarithmic scale. Each data point is recorded for 60 s. The inset illustrates the Jaynes–Cummings ladder structure for the dressed two-level system in a strong laser field that is red-detuned by Δ from the resonance. Four possible transitions are indicated, two of them are frequency degenerate. **b**, Extracted sideband splitting as a function of pump field strength (that is, the square root of the pump power) on a linear scale. The data points exhibit a linear relationship between the square root of the laser power and the sideband splitting (determined by the Rabi frequency). **c**, Zoom-in plot of the 1.852 μW fluorescence spectrum sidebands with a linear intensity scale. The rectangles highlight the sidebands from which we extract a transition linewidth of 343 (±39) MHz.

81 MHz on further fast dephasing mechanisms as determined from $\gamma_{total} = \gamma_{sp} + 2\gamma_{dephasing}$. This suggests that emission from the triplet sidebands of the dressed quantum-dot transition may be at the transform limit. Further first- and second-order coherence experiments on the individual sidebands are necessary to determine the deviation from the Fourier-transform limit for the sideband photons.

In addition to the laser power, the sideband spectrum may also be tuned by the laser frequency. In Fig. 2a, the measured X^{-1} resonance fluorescence spectra, driven by 1.852 μW laser power ($\Omega_b \approx 8\gamma_{sp}$), are plotted for a set of laser-frequency detunings (Δ). For comparison, Fig. 2b shows equation (1) as a function of the laser frequency detuning at fixed laser power. Measuring the spectral separation of the red sideband (when the laser is red-detuned by 2.48 GHz) from the blue sideband (when the laser is blue-detuned by 3.32 GHz) it is possible to achieve photon emission across a frequency band of ∼14 GHz. This is 40 times larger than the 227 MHz spontaneous emission rate, and is by no means an upper limit, but can be further increased by laser power and detuning. To relate this range to other tuning mechanisms, we emphasize that 16 GHz is the range obtainable through d.c. Stark shift of the X^{-1} transition throughout the whole single-electron charging plateau[5]. Alternatively, this is the same frequency shift that each of the two degenerate X^{-1} transitions experiences under an applied magnetic field of 1 T (ref. 26). The sideband splittings extracted from the data set of Fig. 2a are plotted in Fig. 2c as a function of laser detuning. The red fit curve with the functional form of $2\sqrt{\Delta^2 + \Omega_b^2}$ is used to determine a bare Rabi frequency of 2.76±0.2 GHz. From this value, we determine a dipole moment of 27.8±0.2 Debye, in agreement with our differential-transmission measurements.

The final part of this letter is on optical access to a quantum-dot spin, through resonance fluorescence, where a finite magnetic field splits the electronic spin ground states, lifting the X^{-1} spin degeneracy. A reproduction of Fig. 2b under finite magnetic field and accounting for spin is presented in Fig. 3a. The two dressed Zeeman-split sidebands (the blue and red solid lines) are directly correlated to the spin state of the electron and their frequency splitting is controlled by laser detuning beyond that manifested by the magnetic field. In what follows, all frequencies are referenced to the zero-magnetic-field quantum-dot X^{-1} resonance. First, a 50 mT external magnetic field is applied in the Faraday configuration. In Fig. 3b, the fluorescence spectrum of the blue-detuned sideband (the blue rectangle in Fig. 3a) is plotted for laser detunings of 1.75, 1.25 and 0 GHz, from left to right. By varying the laser detuning, at constant power, the Zeeman splitting of the transitions induced by the magnetic field can be altered (Fig. 3b, panels 1 and 2) and even cancelled (Fig. 3b, panel 3).

What we have demonstrated is a combined outcome of the Zeeman and dynamic Stark effect[6,18,27], which enables us to tune independently the energy splitting of the ground and excited states. For InGaAs quantum dots, the electron and hole g-factors are known to be around −0.6 and 1.4 (ref. 26). Therefore, the ground- and excited-state manifolds respond differently to the external magnetic field. The dynamic Stark effect, however,

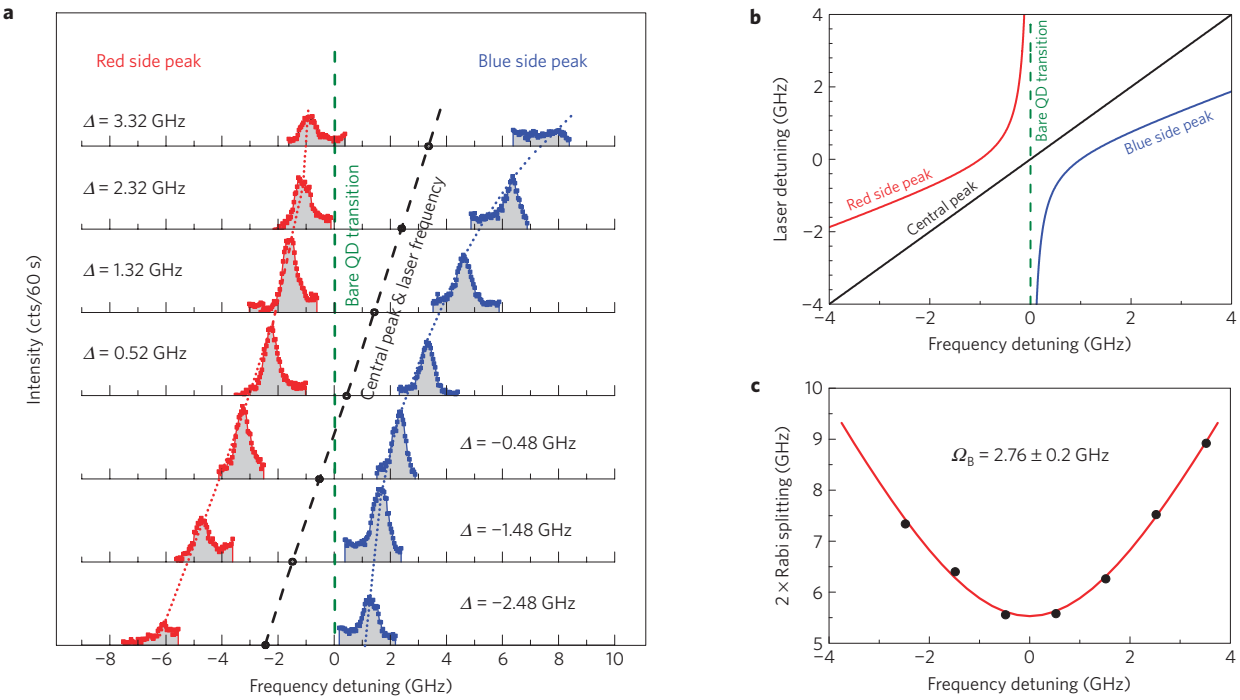

Figure 2 | Dependence of resonance fluorescence on laser detuning. a, Experimentally observed resonance fluorescence spectrum sidebands as a function of laser frequency detuning from the bare X^{-1} resonance at zero magnetic field. The laser power is fixed at 1.852 μW for all detunings. The red and blue dashed curves tracing the sidebands are guides to the eye commensurate with the red and blue curves in **b**. **b**, Simulation of the scattered photon frequencies (red and blue solid curves) for the dressed states of an X^{-1} transition as a function of laser detuning. The dashed green line corresponds to the bare X^{-1} transition and the black dashed line indicates both the laser frequency and the central peak of fluorescence. **c**, Sideband splitting as a function of laser detuning. The bare Rabi frequency of 2.76 GHz and the related transition dipole moment of 27.8 ± 0.2 D are extracted from the fitted red curve.

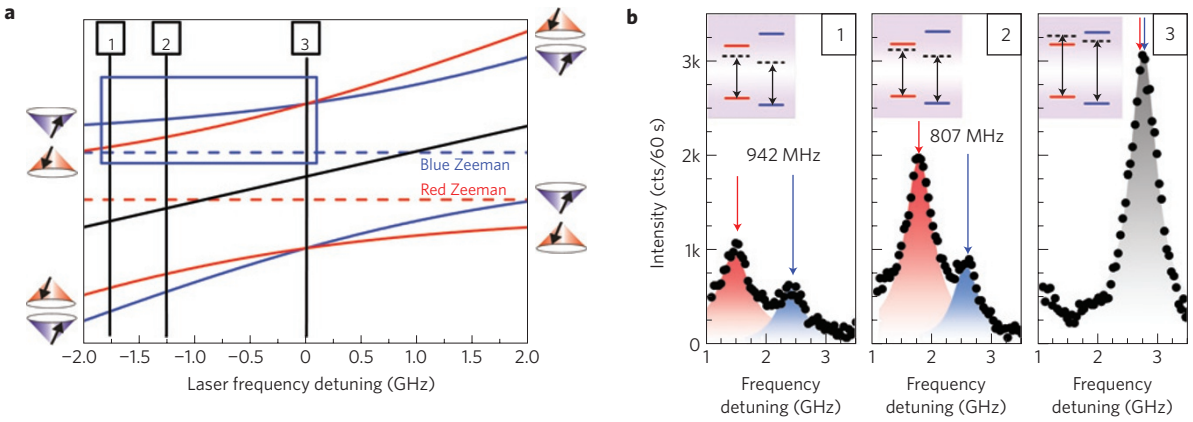

Figure 3 | Spin-selective dynamic Stark effect. a, The simulated scattered photon frequencies for the 1 GHz Zeeman split X^{-1} transitions under a 50 mT external magnetic field. The blue solid lines are the dressed sidebands corresponding to the blue-shifted bare Zeeman transition (dashed blue line) and the red solid lines are the dressed sidebands corresponding to the red-shifted bare Zeeman transition (dashed red line). At the end of each line is an illustration indicating the specific quantum-dot spin ground state for each transition. The blue rectangle and the vertical solid black lines highlight the spectral window and laser detunings relevant for the experimental data shown in **b**. **b**, The evolution of the blue-detuned Mollow sideband spectrum for a series of laser frequency detunings. The inset in the upper left corner illustrates how the laser detunes from the blue (red) Zeeman split transition. The number in the upper right corner designates the corresponding line cut indicated in **a**. The external magnetic field for all spectra is fixed to 50 mT, and the change in spin splitting originates from laser detuning alone.

is independent of either manifold's Landé factor. Consequently, the two state manifolds in this regime exhibit level splittings corresponding to an effective Landé factor tuned by the properties of the laser. The essence of this effect lies in the imbalance of the effective Rabi frequencies ($\Omega = \sqrt{\Delta^2 + \Omega_b^2}$) experienced by the two spin transitions. Here, we use the Δ-dependence to enforce this imbalance and show the cancellation of the magnetic-field-induced spin splitting. The condition given in panel 3 of Fig. 3b is particularly interesting, because both the ground and the excited states are identically split, resulting in an effective Landé factor of 0.4. The consequence is the generation of photons with full spectral overlap, but well-defined spin tags in their circular polarization state for any applied magnetic field strength. This is a regime that merits a thorough investigation for spin–photon entanglement[28].

Finally, laser detuning and magnetic field are used to imprint the spin information onto the resonance fluorescence spectrum

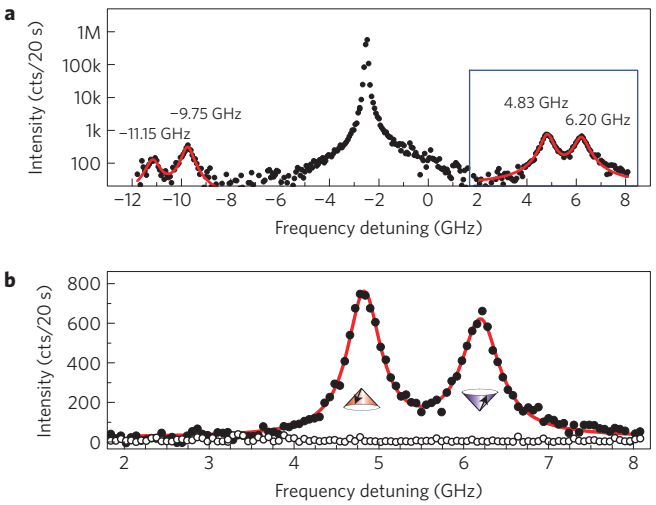

Figure 4 | Mollow quintuplet and spin-resolved fluorescence. a, The full span of the resonance fluorescence spectrum under application of a 100 mT magnetic field and a 2.5 GHz red-detuned laser at a power of 13.2 μW ($\Omega_b \approx 17\gamma_{sp}$) plotted on a linear–log scale (black circles). The number above each sideband peak indicates its central frequency with respect to the bare quantum-dot transition identified as the origin. **b**, A zoom-in of the blue sideband spectrum plotted on a linear–linear scale. The data (filled circles) are fitted to two Lorentzian profiles (red curve) with a splitting of 1.38 GHz. The background is measured for identical conditions without the X^{-1} resonance (open circles).

in the form of a clear, background-free, spectrally distinguished sideband doublet. Figure 4a shows a linear–log plot of the full emission spectrum of another quantum dot under 100 mT magnetic field, 13.2 μW laser power ($\Omega_b \approx 17\gamma_{sp}$) and 2.5 GHz red laser detuning. The plot exhibits a distinctive five-Lorentzian structure in the resonance fluorescence spectrum beyond the previously discussed triplet and each sideband transition is now a clear doublet linked with a quantum-dot electronic spin state. In total there are six features in the spectrum, but, much like the Mollow triplet, the central line comprises two degenerate transitions locked to the detuned laser frequency yielding a spectral signature for the Mollow quintuplet. A zoom-in plot of the blue-sideband doublet, indicated by the blue rectangle, is presented in Fig. 4b on a linear–linear scale. The red curve is a fit of two Lorentzians and the open circles represent the recorded signal in identical conditions except the single electron in the quantum dot is unloaded back to the reservoir eliminating the X^{-1} transitions (the closest possible quantum-dot transition is detuned 1,290 GHz from the laser frequency). This background signal constitutes less than 2% of the total signal. We note here that for all laser powers above 617 nW, when the two sidebands are clearly separable, the total number of photons collected per sideband remains constant, confirming the absence of significant laser background in the above-quoted photon number.

For photonic QIS applications, collection efficiency is as important a factor as spectral purity, so we present an estimate of the photon number collected from the sideband emission. At 13.2 μW excitation power, more than 98% of the emission is coming from the sidebands. Integrating across the blue sideband within the 4 to 7 GHz window (book-keeping for the cavity transmission and detector efficiencies), we estimate that 48,000 photons per second per spin sideband reach the input of our two-mirror cavity. We note that the emission from the two spin sidebands is anticorrelated, determined by the electron spin. Therefore, by matching the cavity transmission spectrum to a spin sideband, quantum-dot spin measurements with above-unity signal-to-noise ratio can be carried out within a time integration of around 1 ms. Although this timescale is already at the threshold of the single-shot spin-readout regime, straightforward technical improvements in the photon collection efficiency[29] will further better this figure of merit.

Propelled by these results, our immediate research directions include the measurement of electronic spin state based on the split sideband detection and the observation of spin quantum jumps. In parallel, the optical tunability and the observation of emission correlations between the two sideband photons (showing the time ordering of the emission due to the Jaynes–Cummings ladder cascade)[30] may serve both as a heralded photon source and as a sensitive spectroscopic probe for weakly coupled states near the original quantum-dot transitions. This step will also be useful when used in conjunction with tunnel-coupled quantum-dot pairs, thus probing more complex ground- and excited-state manifolds. Finally, the modest magnetic field value used in these experiments is chosen to avoid any significant spin pumping and nuclear spin polarization effects, while spectrally resolving the two spin-selective transitions. Therefore, how the emission spectrum of the dressed states evolves when one or both of these mechanisms are significant is an interesting topic of research on its own. Each one of these next steps, if achieved, is expected to have a direct impact on both the pursuit of solid-state QIS and our understanding and control of mesoscopic physical systems.

Methods

The InAs/GaAs quantum dots studied were grown by molecular beam epitaxy and embedded in a Schottky diode heterostructure. An applied gate bias enables deterministic loading of individual electrons[31] from a nearby reservoir (see Supplementary Information, Fig. S1a). The sample is housed in a magneto-optical bath cryostat and cooled to 4.2 K. A cubic zirconia solid immersion lens is used to improve both the light-focusing and light-gathering power of the fibre-based confocal microscope. The differential transmission spectroscopy technique using a scanable single-mode diode laser with 1.2 MHz frequency and 0.5% power stabilization determines the exact spectral location of the X^{-1} transition(s). When the laser is tuned to the X^{-1} transition, resonant scattering from the quantum dot is collected through the second arm of the fibre confocal microscope. The emission is then sent through a moderate-finesse (∼750) two-mirror Fabry–Perot cavity with a 30% throughput at the transmission peak and a 34.5 MHz spectral window of transmission (see Supplementary Information, Figs S2,S3) and subsequently analysed with a liquid-nitrogen-cooled CCD (charge-coupled device). To suppress the background laser light and collect the resonance fluorescence spectrum, we operate the microscope in a dark-field configuration by placing a linear polarizer in the microscope collection arm that is perpendicular to the incoming linearly polarized laser field, providing an extinction of the laser greater than 5×10^3. The excited-state lifetime is obtained from Hanbury–Brown-and-Twiss-type photon-correlation measurements using two single-photon-counting avalanche photodiodes and recording a time-delay coincidence histogram.

Received 29 August 2008; accepted 10 December 2008; published online 25 January 2009; corrected online 1 December 2009

References

1. Nielsen, M. A. & Chuang, I. L. *Quantum Computation and Quantum Information* (Cambridge Univ. Press, 2000).
2. Imamoğlu, A. *et al.* Quantum information processing using quantum dot spins and cavity QED. *Phys. Rev. Lett.* **83,** 4204–4207 (1999).
3. Kroutvar, M. *et al.* Optically programmable electron spin memory using semiconductor quantum dots. *Nature* **432,** 81–84 (2004).
4. Dutt, M. V. G. *et al.* Stimulated and spontaneous optical generation of electron spin coherence in charged GaAs quantum dots. *Phys. Rev. Lett.* **94,** 227403 (2005).
5. Atatüre, M. *et al.* Quantum-dot spin-state preparation with near-unit fidelity. *Science* **312,** 551–553 (2006).
6. Berezovsky, J., Mikkelsen, M. H., Stoltz, N. G., Coldren, L. A. & Awschalom, D. D. Picosecond coherent optical manipulation of a single electron spin in a quantum dot. *Science* **320,** 349–352 (2008).
7. Taylor, J. M., Imamoglu, A. & Lukin, M. D. Controlling a mesoscopic spin environment by quantum bit manipulation. *Phys. Rev. Lett.* **91,** 246802 (2003).
8. Mollow, B. R. Power spectrum of light scattered by two-level systems. *Phys. Rev.* **188,** 1969–1975 (1969).
9. Kim, J., Benson, O., Kan, H. & Yamamoto, Y. Single-photon turnstile device. *Nature* **397,** 500–502 (1999).

10. Michler, P. *et al.* A quantum dot single-photon turnstile device. *Science* **290,** 2282–2285 (2000).
11. Stevenson, R. M. *et al.* A semiconductor source of triggered entangled photon pairs. *Nature* **439,** 179–182 (2006).
12. Yoshie, T. *et al.* Vacuum Rabi splitting with a single quantum dot in a photonic crystal nanocavity. *Nature* **432,** 200–203 (2004).
13. Reithmaier, J. P. *et al.* Strong coupling in a single quantum dot–semiconductor microcavity system. *Nature* **432,** 197–200 (2004).
14. Peter, E. *et al.* Exciton-photon strong-coupling regime for a single quantum dot embedded in a microcavity. *Phys. Rev. Lett.* **95,** 067401 (2005).
15. Knill, E., Laflamme, R. & Milburn, G. J. A scheme for efficient quantum computation with linear optics. *Nature* **409,** 46–52 (2001).
16. Alén, B., Bickel, F., Karrai, K., Warburton, R. J. & Petroff, P. M. Stark-shift modulation absorption spectroscopy of single quantum dots. *Appl. Phys. Lett.* **83,** 2235–2237 (2003).
17. Xu, X. *et al.* Coherent optical spectroscopy of a strongly driven quantum dot. *Science* **317,** 929–932 (2007).
18. Jundt, G., Robledo, L., Högele, A., Fält, S. & Imamoğlu, A. Observation of dressed excitonic states in a single quantum dot. *Phys. Rev. Lett.* **100,** 177401 (2008).
19. Muller, A. *et al.* Resonance fluorescence from a coherently driven semiconductor quantum dot in a cavity. *Phys. Rev. Lett.* **99,** 187402 (2007).
20. Muller, A. *et al.* Coherently driven non-classical light emission from a quantum dot. Preprint at <http://arxiv.org/abs/0707.3808> (2007).
21. Faraon, A. *et al.* Coherent generation of non-classical light on a chip via photon-induced tunnelling and blockade. *Nature Phys.* **4,** 859–863 (2008).
22. Leibfried, D., Blatt, R., Monroe, C. & Wineland, D. Quantum dynamics of single trapped ions. *Rev. Mod. Phys.* **75,** 281–324 (2003).
23. Cohen-Tannoudji, C., Dupont-Roc, J. & Grynberg, G. *Atom-Photon Interactions* (Wiley–Interscience, 1998).
24. Wu, F. Y., Grove, R. E. & Ezekiel, S. Investigation of the spectrum of resonance fluorescence by a monochromatic field. *Phys. Rev. Lett.* **35,** 1426–1429 (1975).
25. Wrigge, G., Gerhardt, I., Hwang, J., Zumofen, G. & Sandoghdar, V. Efficient coupling of photons to a single molecule and the observation of its resonance fluorescence. *Nature Phys.* **4,** 60–66 (2008).
26. Bayer, M. *et al.* Fine structure of neutral and charged excitons in self-assembled In(Ga)As/(Al)GaAs quantum dots. *Phys. Rev. B* **65,** 195315 (2002).
27. Unold, T., Mueller, K., Lienau, C., Elsaesser, T. & Wieck, A. D. Optical stark effect in a quantum dot: Ultrafast control of single exciton polarizations. *Phys. Rev. Lett.* **92,** 157401 (2004).
28. Duan, L.-M. *et al.* Probabilistic quantum gates between remote atoms through interference of optical frequency qubits. *Phys. Rev. A* **73,** 062324 (2006).
29. Vamivakas, A. N. *et al.* Strong extinction of a far-field laser beam by a single quantum dot. *Nano Lett.* **7,** 2892–2896 (2007).
30. Aspect, A., Roger, G., Reynaud, S., Dalibard, J. & Cohen-Tannoudji, C. Time correlations between the two sidebands of the resonance fluorescence triplet. *Phys. Rev. Lett.* **45,** 617–620 (1980).
31. Warburton, R. J. *et al.* Optical emission from a charge-tunable quantum ring. *Nature* **405,** 926–929 (2000).

Acknowledgements

We thank A. Imamoğlu for his continuing support and guidance, S. Fält and A. Badolato for providing high-quality quantum-dot samples and G. Burkard, J. M. Taylor, H. Türeci, A. K. Swan, M. S. Ünlü, B. B. Goldberg and J.-W. Pan for insightful discussions. This work was supported by the University of Cambridge and EPSRC Science and Innovation Awards. A.N.V. is supported by QIPIRC of EPSRC, Y.Z. is supported by the A. v. H. Foundation and LGFG and C.-Y.L. is supported by the University of Cambridge, CSC and CAS.

Additional information

Supplementary information accompanies this paper on www.nature.com/naturephysics. Reprints and permissions information is available online at http://npg.nature.com/reprintsandpermissions. Correspondence and requests for materials should be addressed to A.N.V. or M.A.

CORRIGENDUM

Spin-resolved quantum-dot resonance fluorescence

A. Nick Vamivakas, Yong Zhao, Chao-Yang Lu and Mete Atatüre

Nature Physics **5,** 198–202 (2009); published online: 25 January 2009; corrected after print: 1 December 2009.

The authors wish to point out that in all versions of this Letter originally published, the pure spontaneous emission rate of 356 (±11) MHz quoted on pages 198 and 199 is overestimated by a factor or four owing to an instrumentation-setting error, and erroneously quoted in units of angular frequency. The correct number should read 227 (±7) MHz in linear frequency. The upper bound for fast dephasing mechanisms is therefore limited to 81 MHz, not 18 MHz. The main arguments of the paper are unaffected by this correction. These changes have been made in both PDF and HTML versions of this Letter.